Fullerene-like structures of Cretaceous crinoids reveal topologically limited skeletal possibilities

Jennifer F. Hoyal Cuthill[1,2,3] and Aaron W. Hunter[2,4]

[1]Institute of Analytics and Data Science and School of Life Sciences, University of Essex, Wivenhoe Park, Colchester CO4 3SQ, UK.

[2]Department of Earth Sciences, University of Cambridge, Downing Street, Cambridge, CB2 3EQ

[3] Earth-Life Science Institute, Tokyo Institute of Technology, Tokyo, 152-8550, Japan

[4]School of Earth Sciences, The University of Western Australia, 35 Stirling Highway, Crawley, WA 6009, Australia

There are few cases where numbers or types of possible phenotypes are known, although vast state spaces have been postulated. Rarely applied in this context, graph theory and topology enable enumeration of possible phenotypes and evolutionary transitions. Here, we generate polyhedral calyx graphs for the Late Cretaceous, stemless crinoids *Marsupites testudinarius* and *Uintacrinus socialis* (Uintacrinoidea Zittel) revealing structural similarities to carbon fullerene and fulleroid molecules (respectively). The *U. socialis* calyx incorporates numerous plates (e.g. graph vertices $|V| \geq 197$), which are small, light, low-density and have 4 to 8 sides. Therefore, the corresponding number of possible plate arrangements (number of polyhedral graphs) is large ($>> 1 \times 10^{14}$). Graph vertices representing plates with sides > 6 introduce negative Gaussian curvature (surface saddle points) and topological instability, increasing buckling risk. However, observed numbers of vertices for *Uintacrinus* do not allow more stable pentaradial configurations. In contrast, the *Marsupites* calyx dual graph has 17 faces that are pentagonal or hexagonal. Therefore, it is structurally identical to a carbon fullerene, specifically C30-D5h. Corresponding graph restrictions result in constraint to only

three structural options (fullerene structures C30-C2v 1, C30-C2v 2 and C30-D5h). Further restriction to pentaradial symmetry allows only one possibility: the *Marsupites* phenotype. This robust, stable topology is consistent with adaptation to predation pressures of the Mesozoic marine revolution. Consequently, the most plausible evolutionary pathway between unitacrinoid phenotypes was a mixed heterochronic trade-off to fewer, larger calyx plates. Therefore, topological limitations radically constrained uintacrinoid skeletal possibilities but thereby aided evolution of a novel adaptive phenotype.

Keywords

Evolution, graph theory, echinoderms, morphological state space, morphospace, constraint.

Crinoids are a taxonomic class of extant echinoderms (Ausich *et al.* 1999), first known from the Ordovician Period, branching off early in echinoderm phylogeny (Comeau *et al.* 2017; Wright & Toom 2017) and retaining many characteristics thought to be primitive for the echinoderms as a whole (Oji & Twitchett 2015). Phylogenetically, echinoderms are bilaterians placed in clade Ambulacraria, the sister group to the chordates. Ancestral bilateral symmetry (Zamora *et al.* 2012) is retained today in echinoderm larvae and has been secondarily derived in some groups (e.g. irregular echinoid sea urchins) (Omori *et al.* 2018). However, among many echinoderms, including early crinoids (Guensburg *et al.* 2015; Omori *et al.* 2018), metamorphosis results in a typically pentaradial adult (with fivefold rotational symmetry) arguably the most modified bilaterian body plan (Zamora *et al.* 2012; Byrne *et al.* 2016). Like most other echinoderms, crinoids are primarily (though not exclusively) benthic (living on, or burrowing within, the seafloor). Considering both fossil and extant representatives, most crinoids had a basal holdfast (for attachment to the substrate) and a stalk elevating the calyx, which includes the fixed plates (below the free arms) and contains the major organs and mouth (Ausich *et al.* 1999). However, some show extreme divergence

from this ground-plan. These included the stemless Cretaceous uintacrinoids, of genera *Uintacrinus* and *Marsupites*. These are thought to be closely related, as phylogenetic sister groups (Milsom *et al.* 1994), currently classified as two families Uintacrinidae Zittel, 1879 and Marsupitidae d'Orbigny, 1852 which together form the superfamily Uintacrinoidea (Zittel 1879, placed within order Comatulida (Hess & Messing 2011). Uintacrinoids are closely associated with the chalk substrate of the Cretaceous shallow seas (Table S1). They had a global distribution (Gale *et al.* 1995, 2008) and joint temporal range of ~86−78 Ma, from the Santonian to Campanian stages of the Late Cretaceous period (Gale *et al.* 2008; Hess & Messing 2011), though *Uintacrinus* and the later appearing *Marsupites* coexisted for less than 1 million years (Milsom *et al.* 1994). Both genera possessed long feeding arms and an enlarged, close-to-spherical calyx, composed of 16 large plates in *Marsupites* but many more, small plates in *Uintacrinus* (Figs. 1-2). This expanded calyx is thought to have functioned as a chalk, soft-sediment, stabiliser (Milsom *et al.* 1994; Hess & Messing 2011; Gorzelak *et al.* 2017) or pelagic floatation chamber (Bather 1896; Springer 1901; Seilacher & Hauff 2004). Extreme structural modification into these evolutionarily unusual, free-living forms is, therefore, a potential adaptive response to the soft, chalk substrate conditions of the Cretaceous seas and/or high and increasing (Kerr & Kelley 2015) predation pressure (Meyer & Macurda 1977; Bottjer & Jablonski 1988) of the Mesozoic Marine Revolution (Baumiller *et al.* 2010; Gorzelak *et al.* 2016), a time of marine evolutionary radiation and ecological restructuring (Buatois *et al.* 2016). However, these unusual and functionally controversial morphologies have not previously been analysed within a quantitative framework.

One method which enables the formal analysis and quantification of biological structures such as the crinoid calyx, is the use of graph (network) theory and topology. This falls within the broader field of theoretical (and particularly mathematical) morphology (e.g. pioneered by (Thompson 1942; Raup & Michelson 1965)), which also links to other methods

such as geometric morphometrics (e.g. landmark analysis) and morphospace analyses (which place forms along theoretical spatial axes) (Dera *et al.* 2008; Rasskin-Gutman & Esteve-Altava 2014). Graph theory, specifically, enables enumeration and generation of theoretical structural possibilities for elements (represented by vertices, V) and their connections (represented by edges, E) in a graph ($G = V, E$). Topology additionally considers the geometry of such mathematical structures in physical space (Cromwell 1997). Graph theory and topology provide laws for structures and structural transitions that can be physically realized, with several fundamental theorems initially proposed by Leonhard Euler in the 18th century (Cromwell 1997). Though, so far, comparatively rarely applied to the analysis of biological phenotypes, graph theory has extremely wide potential applicability (as it can be used to evaluate connections between essentially any type of entity) and has been used, for example, to analyse skeletal structures of both invertebrates (including echinoderms (Zachos 2009; Saucède *et al.* 2015)) and vertebrates (Laffont *et al.* 2011).

These techniques therefore enable enumeration of physically possible morphologies, by placing biologically realistic conditions on the types of graphs permitted (as detailed below) and counting the different (non-isomorphic) possibilities. This is particularly valuable because it gives an otherwise rare (Donoghue & Ree 2000) opportunity to explore the number of possible phenotypes (the size of a morphological state space), facilitating the exploration of mathematical and physical constraints on biological evolution (e.g. mathematical or physical limits on the types or numbers of biological forms that are theoretically possible). Enumeration of structural possibilities using graph theory thereby also offers an explicit method to determine the number of possible morphological character states. This is of key utility for new efforts to outline probabilistic models of morphological evolution, for example by forming the denominator for a phylogenetic transition probability (Hoyal Cuthill 2015). The concept of the state space is theoretically linked to that of the morphospace, which (given

101 the definitions of each term above) can be considered as a sub-type of state space which
102 specifically visualises both the number of morphological possibilities and projected locations
103 of given forms within it. A graph theoretic approach has previously been used, for example,
104 to analyse connections between labelled plates of the apical disc, the upper part of the
105 echinoid test (Laffont *et al.* 2011; Saucède *et al.* 2015). A topological approach, additionally
106 considering the properties of graphs when embedded in physical space, has also been used,
107 for example, to model the growth of the echinoid test through life (Zachos 2009).
108 Here, we generate complete, unlabelled graphs of calyx structure for the unusual Late
109 Cretaceous crinoids *Uintacrinus* and *Marsupites*, which we show to have informative
110 structural and topological similarities to the carbon fullerenes, which are polyhedral, trivalent
111 carbon molecules (Schwerdtfeger *et al.* 2015) which, like the calyx of *Marsupites*, have
112 graphs with only pentagonal or hexagonal faces. This graph theoretic approach allows us to
113 enumerate all physically realisable structural alternatives for uintacrinoid skeletons, given
114 biophysically relevant graph conditions of increasing restrictiveness (specifically graphs
115 constrained to be: planar, polyhedral, fullerene and pentameral, with D5h symmetry). This
116 thereby extends previous approaches considering graphs that are not guaranteed to be
117 physically realizable (e.g. planar graphs of isolated parts of the test (Saucède *et al.* 2015)) to
118 enumerate the number of possible graphs that could be actually realized as physical structures
119 (e.g. polyhedral calyces). The latter conditions on the graphs, such as pentameral symmetry
120 in particular, are strongly motivated by modes of echinoderm growth. We then utilise
121 theoretical work on the structure of carbon fullerenes and the related, but often less
122 topologically stable, fulleroid molecules (Schwerdtfeger *et al.* 2015) to discuss the
123 topological stability of alternative calyx skeletal structures and the implications for their
124 function and evolution.
125 **METHOD**

126 *Graph analysis*

127 Graph theoretic analyses were performed to determine possible combinations of skeletal plate
128 adjacencies (structures) for uintacrinoid calyces. This approach considers the number of
129 possible, different (non-isomorphic) arrangements of a given number of plates (i.e. possible
130 calyx structures), without reference to specific spatial locations of plates. These analyses used
131 unlabelled graphs, which represent structures without reference to the identity of individual
132 elements, removing the requirement for plate homologies to be known *a priori* (e.g. (Saucède
133 *et al.* 2015)).

134 *Skeletal graphs*

135 To analyse the possible structural arrangements of uintacrinoid calyces, we modelled
136 calyx theoretical structures using a skeletal graph G ($G = V, E$). This graph has a specified
137 number $|V|$ of vertices V and a corresponding number $|E|$ of edges E (representing potential
138 vertex adjacencies) (Saucède *et al.* 2015). Skeletal graphs were constructed with reference to
139 observations of plate numbers and adjacencies in specific fossil specimens (primarily from
140 the species *Marsupites testudinarius* and *Uintacrinus socialis* Table S1). Each calyx plate
141 was initially represented using a vertex and each plate adjacency represented by an edge
142 connecting the vertices that represent adjacent plates.

143 *Graph constraints*

144 Alternative structural arrangements for uintacrinoid calyces were then enumerated
145 and explored by applying biophysically motivated mathematical conditions on the allowed
146 graphs, which were based on observations of the studied species. To do this, we placed a
147 hierarchical series of mathematical conditions on the skeletal graphs (Table 1), which
148 correspond to biophysical constraints on theoretical calyx structures (combinations of
149 possible plate adjacencies which could be simultaneously realised).

150 *Planar graphs*

A reasonable initial restriction is that echinoderm skeletal graphs should be planar (Saucède *et al.* 2015) (meaning the graph can be embedded on a plane without crossing edges (Schwerdtfeger *et al.* 2015)). A further, biologically realistic and appropriate condition for this analysis of theoretical structural possibilities is that echinoderm skeletal graphs should be simple (unweighted, undirected and without edge loops) and connected (every vertex is connected by an edge to at least one other vertex). The latter condition is required since, articulated skeletons in the studied taxa do not have isolated, disconnected plates.

Polyhedral skeletal graphs

Beyond this, realistic graphs of certain echinoderm skeletal structures should be polyhedral. This includes the enlarged, spheroidal calyces of *Uintacrinus* and *Marsupites*. A polyhedron can be defined simply as a solid, three dimensional shape bounded by a given number of polygonal faces (F) (Cromwell 1997). Through duality, every convex polyhedron with $|F| = n$ faces can be represented by a polyhedral graph with $|V| = n$ vertices and *vice versa* (Duijvestijn & Federico 1981; Grünbaum 2003). A polyhedral graph is simple, 3-vertex-connected (remains connected if fewer than 3 vertices are removed) and planar. Enumeration of all polyhedral graphs with a given number of vertices therefore enables the enumeration of all different structural arrangements which theoretically are physically realizable as polyhedra. Unfortunately, there is no known general formula to calculate the number of possible polyhedral graphs from the number of vertices, edges or faces (Duijvestijn & Federico 1981). However, polyhedral graphs can be constructed algorithmically and counted for specified numbers of vertices (within general computational limits) (Brinkmann & McKay 2007). Other structures such as echinoid tests could also be considered within this framework of polyhedral graph enumeration. For example, polyhedral graphs can map to maximal planar (triangulated) graphs (Stojanović 2016), a computational structure used to model plate growth and movement in developing echinoids (Zachos 2009).

176 Numbers of possible polyhedral graphs (Table 1) were calculated for specified
177 numbers of vertices in the program plantri Version 4.5, Brinkmann and McKay, 2011
178 (https://users.cecs.anu.edu.au/~bdm/plantri/) (Brinkmann & McKay 2007). Plantri
179 algorithmically generates planar graphs under specified conditions and counts the numbers of
180 distinct isomorphism classes. This process is computationally intensive and for larger
181 numbers of plates (Table 1) individual analyses had a run-time of one to two weeks on a
182 desktop PC. The command plantri –p $|V|$ was used to generate all non-isomorphic, 3-
183 connected, planar, simple graphs (convex polytopes), where $|V|$ is the number of vertices in a
184 skeletal graph. The numbers of possible non-isomorphic fullerene graphs and their symmetry
185 groups were enumerated using the plantri command fullgen $|V|$ (Brinkmann & Dress 1997;
186 Brinkmann & McKay 2007).
187 *Dual graphs*
188 For any polyhedral graph, e.g. with vertices representing skeletal plates, a dual graph
189 can be constructed (Schwerdtfeger *et al.* 2015) with vertices representing plate corners. A
190 graph and its dual have the same number of edges. For any polyhedral graph, Euler's formula
191 relates the number of edges ($|E|$), vertices ($|V|$) and faces ($|F|$): $|V| - |E| + |F| = 2$. The skeletal
192 dual graph for *Marsupites*, in which vertices represent plate corners, was constructed in
193 Matlab using a script written by J.F.H.C (Supplementary Computer Code). Graphs were
194 constructed and visualised using the program Gephi (Bastian *et al.* 2009).
195 *Specimen selection and data collection*
196 All available specimens of *Marsupites* and *Uintacrinus* were examined at the Sedgwick
197 Museum of Earth Sciences, University of Cambridge, the Natural History Museum, London
198 and the Booth Museum of Natural History, Brighton. The specimen set on which this study is
199 specifically based comprised thirty well-articulated calyx specimens plus sixty-two
200 disarticulated (isolated) plate specimens (Table S1). Nine, three dimensionally preserved

specimens of *Marsupites* were selected for 3D laser and photosurface scanning using a Next Engine HD Pro scanner at the Sedgwick Museum to aid visualisation and examination of morphology (specimen numbers B24289, B65206, B3871, B3874-75, B3877-78, B3915, B3917).

Plate measurement methodology

Measurements (Tables S-S3) were taken from the 62 disarticulated calyx plates, from *M. testudinarius* or *U. socialis*, held in the Sedgwick Museum of Earth Sciences. Plate thickness was measured using digital calipers with an accuracy of 0.01 mm, with five measurements around the edge used to calculate the average thickness of each plate. The surface area of one side of the plate (outer) was measured from digital photographs using a Matlab script written by J.F.H.C. Plate weight was measured using digital scales with an accuracy of 0.001 g. Plate bounding volume was estimated as upper surface area × thickness. Weight/bounding volume (g/mm^3) was then calculated giving a measure of plate bounding density (which we note is distinct from other possible measures such as internal stereom density e.g. (Gorzelak *et al.* 2017).

Statistical analysis

Statistical analyses of measurements from 62 disarticulated uintacrinoid plates (Table S3, Table S4) were performed using the program Past Paleontological Statistics version 3.14 (Hammer *et al.* 2001). These tested for differences between *M. testudinarius* and *U. socialis* in mean plate thickness (mm), weight (g), area (mm^2), volume (mm^3) and bounding density (weight/bounding volume, g/mm^3). Shapiro-Wilk's tests (Table S4) established whether data were normally distributed (with $p \geq 0.05$). Where data were normally distributed, two-sample t-tests were used to determine if means were significantly different (with $p < 0.05$). Otherwise, non-parametric Mann-Whitney U tests were used to test medians.

RESULTS

Observed variation in skeletal structure

The structure of the calyx in *Marsupites testudinarius* was consistent between observed specimens, consisting of 1 centrale plate, plus 3 plate circlets comprising 5 infrabasal, 5 basal, and 5 radial plates (dicyclic form, with 2 circlets below the radials (Ausich *et al.* 1999)). In contrast, *Uintacrinus socialis* shows intra-specific variability in the number of cup plates (Springer 1901), with 1 to 5 presumed infrabasals reported to be present in approximately half (Rasmussen 1978) of specimens (e.g. Fig. S1) and absent in the remainder (monocylic form, with only 2 cup plate circlets e.g. Fig. 2) (Springer 1901; Rasmussen 1978). In *Marsupites*, the central plate is always approximately pentagonal, followed by sequential circlets of pentagonal infrabasals, hexagonal basals, and radials described as pentagonal (Rasmussen 1978), plus a tegmen opening modelled as pentagonal based on its five radial plate adjacencies (Fig. 1). The consistency of this arrangement gives *Marsupites* its striking structural regularity. However in *Uintacrinus socialis*, plate shape varies strongly, even among plates of the cup (centrale, infrabasal, basals and radials), within and between individuals (Fig. 2, Fig. S1; Plate II of (Springer 1901)). The fixed calyx of *U. socialis* specimen number B11572, for example, contains plates with 4, 5, 6, 7 and 8 sides (Fig. 2). Therefore, fundamental features of calyx structure do not appear to have been fixed within this *Uintacrinus* species or its populations (a phenomenon also observed during extant crinoid development (Comeau *et al.* 2017)). These features include the number of cup circlets, their monocyclic versus dicyclic arrangement, and calyx plate shapes. These detailed observations, primarily from the species *M. testudinarius* and *U. socialis* (Table S1), are consistent with the wider morphological descriptions for these genera (Rasmussen 1978; Hess & Messing 2011), indicating that these observations are informative with regard to the morphological evolution of each genus in its entirety.

Exceptional specimens of *Marsupites* preserve at least 3 (Fig. S2) to 6 (Rasmussen 1978) articulated interbrachial plates between the radials and arms (and 1-3 intersecundibrachs are additionally reported for some specimens) (Rasmussen 1978). Thus in the context of the wider skeleton, the radial plates can be seen to contact at least 7 neighbouring plates (comparable to *Uintacrinus*, Fig. 2), although they remain close to pentagonal in shape (Figs. 1, S2).

Numbers of possible skeletal graphs

Planar graphs

Planar graphs appropriately represent skeletal structures in which plates contact only at their lateral edges (Saucède *et al.* 2015), for example the calyces of the crinoids *Marsupites* and *Uintacrinus*. We note, however, that not all echinoderm skeletons may be realistically represented by planar graphs. For example, clypeasteroid echinoid tests include internal supports which connect oral and apical plates (requiring representation by a non-planar graph) (Nebelsick *et al.* 2015). The number of possible planar graphs is extremely large for even moderate numbers of plate vertices (Table 1).

Polyhedral skeletal graphs

The entire fixed calyx of *Marsupites* has been considered to comprise 16 polygonal cup plates (Milsom *et al.* 1994), with an additional dorsal opening, in life likely covered by a tegmen membrane typical of post-Palaeozoic crinoids. While not found preserved in *Marsupites*, a carbonized tegmen with calcite grains has been observed in *Uintacrinus* (Milsom *et al.* 1994). Frequently, in otherwise well-preserved *Marsupites* fossils, all other plates, above the radials, are disarticulated (e.g. Fig. 1). This calyx structure can therefore be represented using a polyhedral graph (physically realizable as a polyhedron) with 17 vertices and 45 edges (Fig. 1C). Each vertex represents a calyx plate (or the one tegmen) and edges represent their adjacencies. The degree (number of incident edges) of each plate vertex

corresponds both to the number of neighbouring plates and the number of plate sides. Given 17 vertices, the number of possible polyhedral graphs is 6.4×10^{12} (Table 1).

In contrast, the fixed calyx of *Uintacrinus* has been considered to contain far more plates than *Marsupites* (Fig. 2), with fixed brachial plates, up to the 8th secundibrachial, and fixed pinnules, beginning from the 2nd secundibrachial (Milsom *et al.* 1994). Unlike *Marsupites*, articulated *Uintacrinus* fossils are usually flattened so that the complete calyx cannot be viewed in three-dimensions in any single specimen (although many of the specimens available in museum collections are otherwise exceptionally preserved) (Springer 1901). While this makes the precise number of calyx plates difficult to determine with certainty, in any *Uintacrinus* specimen, at least 197 can be inferred based on specimens with exceptionally good preservation (Figs. 2-3, Table S2, Figs. S3-S5). This number of vertices exceeds general computational limit for algorithmic generation of polyhedral graphs (Brinkmann & McKay 2007). However, at 18 plate vertices (for comparison against the 17 vertices for *Marsupites*) the number of possible polyhedral graphs is already 1×10^{14} (Table 1), showing that the space of possible polyhedral graph structures becomes far larger for calyx plate numbers exceeding those of *Marsupites*.

The number of possible polyhedral graphs therefore remains very large (> 6 trillion) for uintacrinoid calyx graphs (Table 1). However, applying this biologically realistic condition nonetheless reveals an enormous narrowing of structural possibilities. Relative to the vast state-space of planar graphs, restriction to polyhedral graphs leads to a reduction of at least 13 in the order of magnitude of the state space (Table 1).

Fullerene graphs

The *Marsupites* calyx graph (Fig. 1C, Table S5) has 17 plate vertices and 45 edges. This specific graph has been studied in other mathematical contexts where it is known as the Errera graph (Hutchinson & Wagon 1998). Its dual graph (Fig. 1D, Table S6) is a polyhedral,

301 trivalent graph (in which each vertex has degree 3), with 17 faces, 30 vertices and 45 edges
302 (Fig. 1D). This graph also represents a carbon fullerene molecule, C30-D5h, which has a
303 single fivefold rotational symmetry axis (D5 symmetry group) and a perpendicular mirror
304 plane (D5h symmetry group (Cromwell 1997)). There are three possible, non-isomorphic
305 fullerene graphs with 30 vertices (Table 1, fullerenes C30-C2v 1, C30-C2v 2 and C30-D5h,
306 with the two fullerenes of group C2v having twofold symmetry).

307 The calyx of *U. socialis* contains plates with 4 to 8 sides (Figs. 2-3, Table S7).
308 Therefore, not all fixed calyx plates are pentagons or hexagons. Consequently, the
309 *Uintacrinus* calyx dual graph is more comparable to a fulleroid graph (which allows faces
310 with any number of sides greater than 5 (Kardoš 2007; Schwerdtfeger *et al.* 2015), although
311 occasional plates with four sides (e.g. Figs. 2, S3) deviate from an exact correspondence with
312 fulleroid structures. With the condition of only pentagonal or hexagonal faces removed, the
313 number of possible skeletal structures can again be considered using the number of possible
314 polyhedral graphs (Table 1).

315 *Measurements of plate size, weight and density*

316 Measurements of 62 disarticulated calyx plates showed that, on average, plates of *U.*
317 *socialis* were significantly smaller than those of *M. testudinarius* in terms of area, thickness
318 and estimated volume. They were also lighter in weight and lower in estimated bounding
319 density (weight/bounding volume, g/mm^3, Table S3).

320 **DISCUSSION**

321 *Comparisons between Uintacrinus and Marsupites*

322 *Marsupites* and *Uintacrinus* show marked similarities in overall skeletal structure.
323 These similarities include the presence of articulated interbrachial plates in exceptional
324 specimens of *Marsupites*, which are therefore comparable in location and numbers of
325 contacts to those fixed into the calyx of *Uintacrinus*. Indeed, Rasmussen grouped these

interbrachials of *Marsupites* as calyx plates, while noting that they met the brachials with loose sutures. Furthermore, among some, and particularly small, specimens of *Uintacrinus socialis*, the number of fixed interbrachial calyx plates (below the first fixed pinnules) is comparatively low, overlapping that seen in *Marsupites* (e.g. 5-6 in Plate VI Fig. 4 of (Springer 1901)). In contrast, other, larger specimens show a greater number of interbrachials, as well as interradials. For example, 12 interbrachials are visible below the first fixed pinnule in *U. socialis* specimen B11572 (Fig. 2). This indicates a growth trajectory in which interbrachial plates continue to be added during growth and development throughout life (Springer 1901; Rasmussen 1978). The structure of the arms is also similar in the two genera, supporting a close phylogenetic relationship (Milsom *et al.* 1994), with arms branching once at the same inferred position (the second primibrach (Rasmussen 1978)), and complete pinnulation reported from the outer 2nd secundibrachs (Rasmussen 1978; Milsom *et al.* 1994) (although pinnules are not as well preserved in even well-articulated *Marsupites* fossils, e.g. Fig. S2, as in *Uintacrinus*, e.g. Fig. 2).

However, *Marsupites* and *Uintacrinus* show contrasting strategies in the composition of the fixed calyx. *Uintacrinus* has a fixed calyx of greater maximum size (at ≤ 75 mm in diameter (Rasmussen 1978)) with more plates, while individual plates are smaller, lighter and less dense (weight/bounding volume, g/mm^3, Table S3). The slightly smaller calyx of *Marsupites* (at ≤ 60 mm in diameter (Rasmussen 1978)) is instead mainly composed of considerably larger and more robust cup plates (Fig. 1). For example, the cup plates represent approximately 20% of the distance between the centrale and distal interbrachial (below the first fixed pinnule) in *U. socialis* (Fig. 2), but 80% in *M. testudinarius* (Fig. S2). The two genera also differ in the structure of the calyx cup, which is fixed to a dicyclic arrangement in *Marsupites* (with 2 plate circlets below the radials (Ausich *et al.* 1999) but polymorphic, with both monocyclic (1 sub-radial plate circlet) and dicyclic arrangements present in *Uintacrinus*

(Rasmussen 1978), even among intraspecific specimens (e.g. of *U. socialis*) from the same locality (Springer 1901).

Uintacrinoid calyx graphs and similarity to carbon fullerenes

Fullerenes are carbon molecules in which each carbon atom bonds to 3 others, forming cage-like structures with often near-spherical, polyhedral shapes (such as C_{60}, buckminsterfullerene) (Schwerdtfeger *et al.* 2015). Therefore, fullerene graphs are trivalent graphs (each vertex has 3 incident edges) composed of only pentagon and hexagon faces (Schwerdtfeger *et al.* 2015), as is the *Marsupites* calyx. Consequently, the same graph (Fig. 1D) represents both the carbon fullerene C_{30}-D5h (with 30 vertices representing carbon atoms) and the calyx of *Marsupites* (with 30 vertices representing plate corners).

These observations allow us to explore counterfactual possibilities for calyx structure. For example, we might ask how many pentagonal versus hexagonal plates *Marsupites* could have, while maintaining the observed composition of only pentagons or hexagons. In fact, there is only one possible composition. According to Euler's theorem there must be exactly 12 pentagons in any polyhedron composed of only pentagons or hexagons (Schwerdtfeger *et al.* 2015). Twelve is, therefore, the number of pentagonal plates observed in the *Marsupites* calyx (with 1 centrale, 5 infrabasals, 5 radials, closed by the 1 tegmen opening, each with 5 sides (Rasmussen 1978)). This results from Euler's polyhedral formula ($|V| - |E| + |F| = 2$). From this we can also see that, for a polyhedron with 17 faces which are either pentagons or hexagons, there must be exactly 5 hexagons (17 - 12 = 5). Correspondingly, 5 hexagonal basal plates are observed in *Marsupites*, and can also be seen in other dicyclic crinoids including some specimens of *Uintacrinus* and the cladid *Eoparisocrinus siluricus* (e.g. Fig. 28 of (Ausich *et al.* 1999)). Given only pentagonal and hexagonal plates, other compositions, for example a polyhedral calyx made up of 17 pentagonal plates, are simply not physically possible.

We can then ask how many combinatorially different ways there are to make a polyhedron composed of 12 pentagonal and 5 hexagonal faces. This corresponds to the number of possible, non-isomorphic fullerene graphs with 30 vertices, which is just 3 (fullerenes C30-C2v 1, C30-C2v 2 and C30-D5h). Of these, the number with 5-fold rotational symmetry is one (the D5h symmetry group, with the two fullerenes of group C2v having twofold symmetry). This is the structure observed for the calyx of *Marsupites* and the fullerene C30-D5h. While pentaradial symmetry is not universal among echinoderms, it is ancient (established by the early Cambrian (Smith & Zamora 2013)) and widely expressed, for example in the frequent occurrence of 5 radials, 5 arms, 5 water vascular canals, 5 ambulacral food grooves, and 5 oral plates (Rasmussen 1978; Ausich *et al.* 1999), indicating a strong constraint on echinoderm morphology throughout most of their evolutionary history.

The calyx of *U. socialis* was observed to contain plates with 4 to 8 sides (Figs. 2-3, Table S7). Therefore, not all fixed calyx plates are pentagons or hexagons (as was the case for *Marsupites*). The total number of pentagonal plates (e.g. 63 in Fig. 3) also greatly exceeds the 12 allowed for fullerene dual graphs. Consequently, the dual graph for the *U. socialis* calyx is more comparable to a fulleroid graph, a generalisation of a fullerene graph to allow faces with any number of sides greater than 5 (Kardoš 2007; Schwerdtfeger *et al.* 2015). However, we note that *U. socialis* calyces were observed to have occasional plates with four sides (e.g. Figs. 2, S3) thereby deviating from an exact correspondence with fulleroid structures. Without the restriction to only pentagonal or hexagonal faces (which was observed in *Marsupites* but not *Uintacrinus*), the number of possible calyx structures for *Uintacrinus* corresponds to the number of possible polyhedral graphs, with a consequent increase in the number of structural possibilities compared to fullerene graphs only (Table 1).

The introduction of vertices with greater than 6 sides in the calyx of *Uintacrinus* causes negative Gaussian curvature (the product of the minimal and maximal curvatures

around a point). Negative Gaussian curvature, which gives the calyx graph a wavy surface with saddle-shaped areas (Figs. 2-3), reduces structural stability (Schwerdtfeger *et al.* 2015) for example due to uneven distribution of strain which can cause local buckling (Liang & Mahadevan 2009). In line with this expectation from topological principles, the calyx of *Marsupites* (which has a topologically stable fullerene structure) is often preserved three-dimensionally (e.g. Fig. 1) whereas for *Uintacrinus* (which shows more topologically unstable structures) all articulated calyces held in the examined museum collections were crushed flat (e.g. Fig. 2). This difference in topological stability is particularly notable given that the Cretaceous was a time when new crushing predators such as crabs were diversifying (Tsang *et al.* 2014). The calyx provides the external protection for all major organs of the crinoid and its structural integrity is of vital importance. Why does the calyx of *Uintacrinus* not then consist of a topologically more stable combination of only pentagonal and hexagonal plates, analogous to large fullerene molecules? An answer emerges from the mathematical properties of polyhedra (as well as the echinoderm plate addition process). For some numbers of vertices equal to or less than those observed in *Uintacrinus* (Table 1), not all possible fullerenes have a 5-fold rotational symmetry axis (e.g. C30-C2v discussed above), additional perpendicular mirror plane (D5h symmetry group), or even any symmetry axis at all (e.g. the C1 symmetry group (Cromwell 1997)). Structures without D5 symmetry are incompatible with plate addition that maintains the pentameral rotational axis dominant among echinoderms. Structures without D5h symmetry will also lack the mirror symmetry seen along the oral-aboral axis of the *Marsupites* calyx. Unlike *M. testudinarius* (in which all studied specimens had the same complement of calyx plates), *U. socialis* specimens appear to have continued to add calyx plates throughout life. Therefore large numbers of plates, as observed in the calyx of *Uintacrinus* (Table 1), preclude the possession and continuous maintenance of a biologically appropriate fullerene structure.

426 *Evolutionary and Functional Implications*

427 Based on these observations and graph theoretic analyses, we can evaluate the most
428 likely evolutionary pathways to uintacrinoid morphologies. This is conceptually equivalent to
429 reconstructing character states for the hypothetical ancestor of *Uintacrinus* and *Marsupites*,
430 within a phylogenetic framework involving consideration of state transition probabilities.
431 Given the evidence for continued plate addition throughout life, it is developmentally
432 plausible that *Uintacrinus* represents an extreme extension of an ontogenetic trajectory of
433 calyx plate addition, with a large number of smaller, lighter plates conferring a highly
434 spherical, lightweight calyx. Such adaptations are compatible with both previously proposed
435 functions, either as a benthic stabiliser on soft sediment (Milsom *et al.* 1994; Hess & Messing
436 2011; Gorzelak *et al.* 2017) or pelagic floatation chamber (Bather 1896; Springer 1901;
437 Seilacher & Hauff 2004). However, we show that in *Uintacrinus* (relative to *Marsupites*)
438 calyx expansion occurred by increased plate number despite a cost to structural stability. This
439 emphasises the importance of an exceptionally large and lightweight calyx to *Uintacrinus*,
440 potentially providing a point in favour of a free-living, pelagic habit for this genus (Bather
441 1896; Springer 1901; Seilacher & Hauff 2004). In addition, some calyx plates of *Uintacrinus*
442 show deep excavations and asymmetric thickening (Fig. S6), reducing their average bounding
443 density (weight/bounding volume, g/mm^3, Table S3) and therefore the overall weight of the
444 calyx.

445 Relative to *Uintacrinus*, *Marsupites* represents a reduction in calyx plate number at
446 maturity, indicating possible evolution by paedomorphic heterochrony (evolution in the
447 timing of development, i.e. heterochrony, that produces juvenile-like characteristics in the
448 adult (McNamara 1986)). Alongside this reduction in plate number, *Marsupites* also displays
449 comparatively extended growth of individual plates, a possible example of peramorphic
450 heterochrony (evolution that increases the relative extent of development in the adult

(McNamara 1986)). Overall, therefore, mixed heterochrony (Alba 2002) could have resulted in a more robust calyx composed of fewer, larger plates, via modification of the timing of developmental processes of plate addition and growth that were inherited from their most recent common ancestor and/or are shared more widely among crinoids and other echinoderms (Comeau *et al.* 2017). Further to this, topological considerations suggest that the fixed calyx of *Marsupites* is more structurally stable than that of *Uintacrinus*, which exhibits negative Gaussian curvature. Moreover, the reduction in maximum calyx plate number in *Marsupites* relative to *Uintacrinus* leads to a radical decrease in the number of structural possibilities and a differing number of stable options (Table 1). Specifically, a transition from the large number of calyx plates observed in *Uintacrinus* to the small number observed in *Marsupites* results in a comparatively high probability that a topologically stable fullerene structure with pentaradial symmetry is available e.g. 1 in 3 considering all possible fullerene graphs (Table 1). In contrast, a transition in the opposite direction (from a small to large number of calyx plates) can result in a zero probability of accessing a stable fullerene structure with pentaradial symmetry (Table 1). Therefore, a simple reduction in calyx plate number would have made the evolution of the more stable structural configuration of *Marsupites* relatively likely on probabilistic grounds.

In general, biological evolution is capable of remarkable increases in complexity (Szathmáry and Smith 1995), although decreases in complexity often occur when opposing selection pressures are reduced (with evolutionary reductions in parasites and cave-dwelling fish providing famous examples (Porter & Crandall 2003)). Indeed, both *Uintacrinus* and *Marsupites* possessed a calyx structure which is larger and, in *Uintacrinus* at least, considerably more complex than their previously inferred phylogenetic sister-group (Milsom *et al.* 1994), the comatulid crinoid genus *Comatula* (which also shows a highly reduced stalk). This indicates, for example, that evolution of the shared uintacrinoid morphology

476 involved an increase in the number of adult cup plate circlets from the monocylic form in
477 adult comatulids (larvally dicyclic), to polymorphic dicyclic/monocyclic forms in adult
478 *Uintacrinus* and stably dicyclic form in *Marsupites*. However, with regard to the principal
479 difference between *Uintacrinus* and *Marsupites* calyx morphologies (the number of non-cup
480 plates incorporated into the calyx), we show that an increase in calyx plate number and,
481 consequently, structural complexity is accompanied by a decrease in the number of
482 topologically stable options (Table 1). Consequently, on mathematical and biophysical
483 grounds, the probability of forward transition (from the absence to presence of fixed
484 interradial calyx plates) might be considered to be lower than the probability of backward
485 transition (to the less complex and more stable calyx configuration, lacking fixed
486 interradials). This would then support a *Uintacrinus*-like ancestral morphology for the
487 uintacrinoids. This is consistent with an increase in the structural strength of the calyx in
488 *Marsupites*, and potentially a concomitant return to a more benthic life-habit (Milsom *et al.*
489 1994; Hess & Messing 2011; Gorzelak *et al.* 2017), in response to Late Cretaceous predation
490 pressures during the 'Mesozoic Marine Revolution'. The alternative, under equal transition
491 probabilities (though less consistent with a monocylic-polymorphic-dicyclic cup transition),
492 would suggest that the *Marsupites* morphology was ancestral, with *Uintacrinus* as a
493 secondary attempt at even more extreme calyx expansion, despite the associated costs to
494 structural stability. Ultimately, both of these unique morphological strategies were to
495 disappear with the extinction of both *Uintacrinus* and *Marsupites* by the late Campanian
496 stage of the Late Cretaceous Period (Gale *et al.* 2008; Hess & Messing 2011).
497

498 **REFERENCES**

499 ALBA, D. M. 2002. Shape and stage in heterochronic models. *In Human Evolution through*
500 *Developmental Change*, The John Hopkins University Press, Baltimore and London.
501 AUSICH, W. I., BRETT, C. E., HESS, H. and SIMMS, M. J. 1999. Crinoid form and
502 function. *In Fossil Crinoids*, Cambridge University Press, Cambridge, 3–30 pp.

BASTIAN, M., HEYMANN, S. and JACOMY, M. 2009. Gephi: an open source software for exploring and manipulating networks. *Icwsm*, **8**, 361–362.
BATHER, F. A. 1896. On *Uintacrinus*: a morphological study. *Proceedings of the Zoological Society of London*, 974–1003.
BAUMILLER, T. K., SALAMON, M. A., GORZELAK, P., MOOI, R., MESSING, C. G. and GAHN, F. J. 2010. Post-Paleozoic crinoid radiation in response to benthic predation preceded the Mesozoic marine revolution. *Proceedings of the National Academy of Sciences*, **107**, 5893–5896.
BONICHON, N., GAVOILLE, C., HANUSSE, N., POULALHON, D. and SCHAEFFER, G. 2006. Planar graphs, via well-orderly maps and trees. *Graphs and Combinatorics*, **22**, 185–202.
BOTTJER, D. J. and JABLONSKI, D. 1988. Paleoenvironmental patterns in the evolution of post-Paleozoic benthic marine invertebrates. *Palaios*, **3**, 540–560.
BRINKMANN, G. and DRESS, A. W. 1997. A constructive enumeration of fullerenes. *Journal of Algorithms*, **23**, 345–358.
——— and MCKAY, B. D. 2007. Fast generation of planar graphs. *MATCH Communications in Mathematical and in Computer Chemistry*, **58**, 323–357.
BUATOIS, L. A., CARMONA, N. B., CURRAN, H. A., NETTO, R. G., MÁNGANO, M. G. and WETZEL, A. 2016. The Mesozoic marine revolution. *In The Trace-Fossil Record of Major Evolutionary Events*, Springer, 19–134 pp.
BYRNE, M., MARTINEZ, P. and MORRIS, V. 2016. Evolution of a pentameral body plan was not linked to translocation of anterior Hox genes: the echinoderm HOX cluster revisited. *Evolution & Development*, **18**, 137–143.
COMEAU, A., BISHOP, C. D. and CAMERON, C. B. 2017. Ossicle development of the crinoid Florometra serratissima through larval stages. *Canadian Journal of Zoology*, **95**, 183–192.
CROMWELL, P. R. 1997. *Polyhedra*. Cambridge University Press, Cambridge.
DERA, G., EBLE, G. J., NEIGE, P. and DAVID, B. 2008. The flourishing diversity of models in theoretical morphology: from current practices to future macroevolutionary and bioenvironmental challenges. *Paleobiology*, **34**, 301–317.
DONOGHUE, M. J. and REE, R. H. 2000. Homoplasy and developmental constraint: a model and an example from plants. *American Zoologist*, **40**, 759–769.
DUIJVESTIJN, A. J. W. and FEDERICO, P. J. 1981. The number of polyhedral (3-connected planar) graphs. *Mathematics of Computation*, **37**, 523–532.
GALE, A. S., MONTGOMERY, P., KENNEDY, W. J., HANCOCK, J. M., BURNETT, J. A. and MCARTHUR, J. M. 1995. Definition and global correlation of the Santonian-Campanian boundary. *Terra Nova*, **7**, 611–622.
GALE, A. S., HANCOCK, J. M., KENNEDY, W. J., PETRIZZO, M. R., LEES, J. A., WALASZCZYK, I. and WRAY, D. S. 2008. An integrated study (geochemistry, stable oxygen and carbon isotopes, nannofossils, planktonic foraminifera, inoceramid bivalves, ammonites and crinoids) of the Waxahachie Dam Spillway section, north Texas: a possible boundary stratotype for the base of the Campanian Stage. *Cretaceous Research*, **29**, 131–167.
GORZELAK, P., SALAMON, M. A., TRZĘSIOK, D., LACH, R. and BAUMILLER, T. K. 2016. Diversity dynamics of post-Palaeozoic crinoids–in quest of the factors affecting crinoid macroevolution. *Lethaia*, **49**, 231–244.
GORZELAK, P., GLUCHOWSKI, E., BRACHANIEC, T., LUKOWIAK, M. and SALAMON, M. A. 2017. Skeletal microstructure of uintacrinoid crinoids and inferences about their mode of life. *Palaeogeography, Palaeoclimatology, Palaeoecology*, **468**, 200–207.

GRÜNBAUM, B. 2003. *Convex polytopes*. Springer-Verlag, New York.
GUENSBURG, T. E., BLAKE, D. B., SPRINKLE, J. and MOOI, R. 2015. Crinoid ancestry without blastozoans. *Acta Palaeontologica Polonica*, **61**, 253–266.
HAMMER, Ø., HARPER, D. A. T. and RYAN, P. D. 2001. PAST: Paleontological Statistics Software Package for Education and Data Analysis. *Electron*, **4**, 9.
HESS, H. and MESSING, C. G. 2011. Treatise on Invertebrate Paleontology, Part T, Echinodermata 2 Revised, Crinoidea 3. *In Lawrence, University of Kansas and Paleontological Institute*, 216 pp.
HOYAL CUTHILL, J. F. 2015. The morphological state space revisited: what do phylogenetic patterns in homoplasy tell us about the number of possible character states? *Interface focus*, **5**, 20150049.
HUTCHINSON, J. and WAGON, S. 1998. Kempe Revisited. *The American Mathematical Monthly*, **105**, 170–174.
KARDOŠ, F. 2007. Tetrahedral Fulleroids. *Journal of Mathematical Chemistry*, **41**, 101–111.
KERR, J. P. and KELLEY, P. H. 2015. Assessing the influence of escalation during the Mesozoic Marine Revolution: shell breakage and adaptation against enemies in Mesozoic ammonites. *Palaeogeography, Palaeoclimatology, Palaeoecology*, **440**, 632–646.
LAFFONT, R., FIRMAT, C., ALIBERT, P., DAVID, B., MONTUIRE, S. and SAUCÈDE, T. 2011. Biodiversity and evolution in the light of morphometrics: From patterns to processes. *Comptes Rendus Palevol*, **10**, 133–142.
LIANG, H. and MAHADEVAN, L. 2009. The shape of a long leaf. *Proceedings of the National Academy of Sciences of the United States of America*, **106**, 22049–22054.
MCNAMARA, K. J. 1986. A guide to the nomenclature of heterochrony. *Journal of Paleontology*, **60**, 4–13.
MEYER, D. L. and MACURDA, D. B. 1977. Adaptive radiation of the comatulid crinoids. *Paleobiology*, **3**, 74–82.
MILSOM, C. V., SIMMS, M. J. and GALE, A. S. 1994. Phylogeny and palaeobiology of *Marsupites* and *Uintacrinus*. *Palaeontology*, **37**, 595–608.
NEBELSICK, J. H., DYNOWSKI, J. F., GROSSMANN, J. N. and TÖTZKE, C. 2015. Echinoderms: hierarchically organized light weight skeletons. *In Evolution of Lightweight Structures*, Springer, 141–155 pp.
OJI, T. and TWITCHETT, R. J. 2015. The oldest post-Palaeozoic Crinoid and Permian-Triassic origins of the Articulata (Echinodermata). *Zoological Science*, **32**, 211–215.
OMORI, A., KIKUCHI, M. and KONDO, M. 2018. Larval and Adult Body Axes in Echinoderms. *In* KOBAYASHI, K., KITANO, T., IWAO, Y. and KONDO, M. (eds.) *Reproductive and Developmental Strategies: The Continuity of Life*, Springer Japan, Tokyo, 763–789 pp.
PORTER, M. L. and CRANDALL, K. A. 2003. Lost along the way: the significance of evolution in reverse. *Trends in Ecology & Evolution*, **18**, 541–547.
RASMUSSEN, H. W. 1978. Articulata-Uintacrinida. *In Treatise on Invertebrate Paleontology. Part T: Echinodermata 2 (Crinoidea)*, Boulder, T813–T1027 pp.
RASSKIN-GUTMAN, D. and ESTEVE-ALTAVA, B. 2014. Connecting the Dots: Anatomical Network Analysis in Morphological EvoDevo. *Biological Theory*, **9**, 178–193.
RAUP, D. M. and MICHELSON, A. 1965. Theoretical morphology of the coiled shell. *Science*, **147**, 1294–1295.
SAUCÈDE, T., LAFFONT, R., LABRUÈRE, C., JEBRANE, A., FRANÇOIS, E., EBLE, G. J. and DAVID, B. 2015. Empirical and theoretical study of atelostomate (Echinoidea,

Echinodermata) plate architecture: using graph analysis to reveal structural constraints. *Paleobiology*, **41**, 436–459.
SCHWERDTFEGER, P., WIRZ, L. N. and AVERY, J. 2015. The topology of fullerenes. *Wiley Interdisciplinary Reviews: Computational Molecular Science*, **5**, 96–145.
SEILACHER, A. and HAUFF, R. B. 2004. Constructional morphology of pelagic crinoids. *Palaios*, **19**, 3–16.
SMITH, A. and ZAMORA, S. 2013. Cambrian spiral-plated echinoderms from Gondwana reveal the earliest pentaradial body plan. *Proceedings of the Royal Society of London B*, **280**, 20131197.
SPRINGER, F. 1901. Uintacrinus: its structure and relations. *Memoirs of the Museum of Comparative Zoölogy at Harvard College*, **25**, 1–89.
STOJANOVIĆ, M. 2016. Convex polyhedra with triangular faces and cone triangulation. *Yugoslav Journal of Operations Research*, **21**, 79–92.
THOMPSON, D. W. 1942. *On growth and form*. Cambridge University Press, Cambridge.
TSANG, L. M., SCHUBART, C. D., AHYONG, S. T., LAI, J. C. Y., AU, E. Y. C., CHAN, T.-Y., NG, P. K. L. and CHU, K. H. 2014. Evolutionary history of true crabs (Crustacea: Decapoda: Brachyura) and the origin of freshwater crabs. *Molecular Biology and Evolution*, **31**, 1173–1187.
WRIGHT, D. F. and TOOM, U. 2017. New crinoids from the Baltic region (Estonia): fossil tip-dating phylogenetics constrains the origin and Ordovician–Silurian diversification of the Flexibilia (Echinodermata). *Palaeontology*, **60**, 893–910.
ZACHOS, L. G. 2009. A new computational growth model for sea urchin skeletons. *Journal of Theoretical Biology*, **259**, 646–657.
ZAMORA, S., RAHMAN, I. A. and SMITH, A. B. 2012. Plated Cambrian bilaterians reveal the earliest stages of echinoderm evolution. *PLoS One*, **7**, e38296.

FIGURE CAPTIONS

Figure 1. Calyx graphs for the Cretaceous crinoid *Marsupites testudinarius*. Aboral (**A**) and lateral (**B**) views, from laser and photosurface scans of Sedgwick Museum of Earth Sciences specimen number B24289, Upper Chalk, UK. Scale bar 1 cm (**B**). Letters indicate plate names: C centrale, I infrabasal, B basal, R radial, T tegmen opening. Unlabelled graph (**C**) and dual graph (**D**) of calyx structure. (**C**) 17 vertices (white-filled circles) represent the 16 calyx plates and tegmen. (**D**) 30 vertices (black circles) represent plate corners. The 45 connecting edges (lines) represent vertex adjacencies. The *Marsupites* calyx dual graph (**D**) has the same structure as the carbon fullerene molecule C_{30}-D5h and all faces are pentagons or hexagons. For visualisation, graph vertices (**C-D**) were positioned using a Yifan-Hu layout in the program Gephi (Bastian *et al.* 2009).

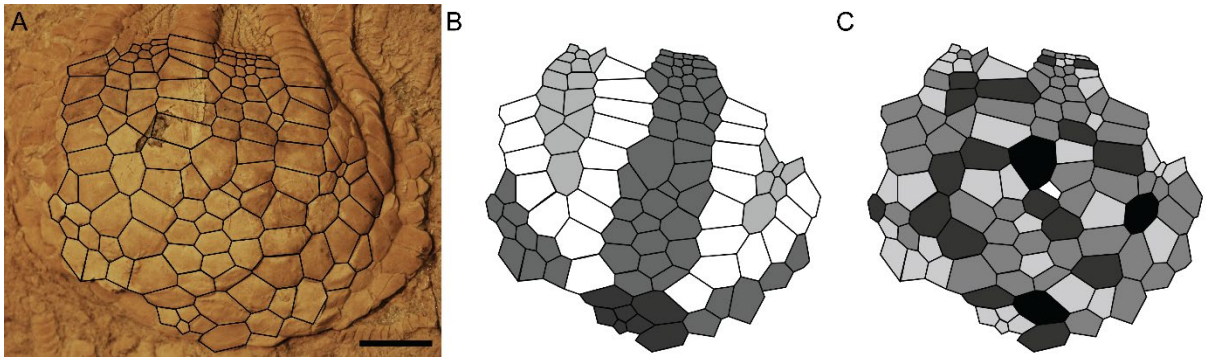

Figure 2. Calyx of *Uintacrinus socialis*. (**A**) Photograph of Sedgwick Museum of Earth Sciences specimen number B11572, Niobrara Chalk, USA, with diagram of plates. Scale bar 1 cm. (**B**) Plate types: cup dark grey, fixed brachials (arms) white, interbrachials/fixed pinnules mid grey, interradials/fixed pinnules light grey. (**C**) Number of sides of each plate: 4 white, 5 light grey, 6 mid grey, 7 dark grey, 8 black.

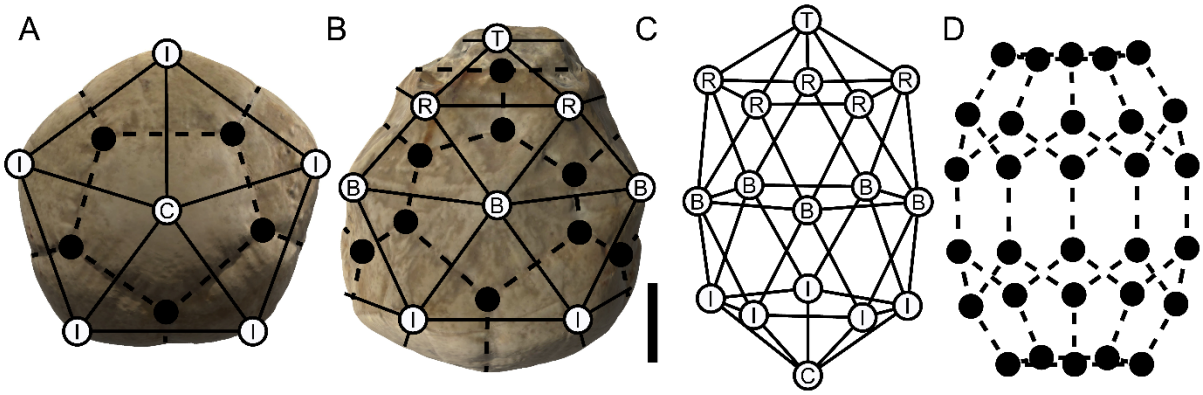

Figure 3. Calyx graph for juvenile *Uintacrinus socialis* (A). The calyx graph has a total of 197 vertices, representing plates, and 585 edges, representing plate adjacencies. (**B**) Vertex degrees correspond to numbers of plate adjacencies and sides (with all vertices included). (**A**) Graph visualisation, vertex positions generated as for Fig. 1. Tegmen vertex and its 40 incident edges removed for visual clarity (vertex colours show degree with all vertices included; Table S7). Plate adjacency pattern based on examination of specimens 1, (Springer 1901) plate VI fig. 4, 2, B11572 (Fig. 2) and 3 (Figs. S3-S4). Adjacency patterns inferred

from individual 2D compressed specimens (maximum 2 interambulacral regions visible) combined and rotationally duplicated to close graph in 3D. Cup structure based on specimens 1-3 (extent of fixed calyx 1, aboral interbrachials and interradials 1-2, fixed pinnules 3). Double size nodes (and colour version, red outlines) indicate plates incorporated into the fixed calyx of *Marsupites* and cup of *Uintacrinus*.

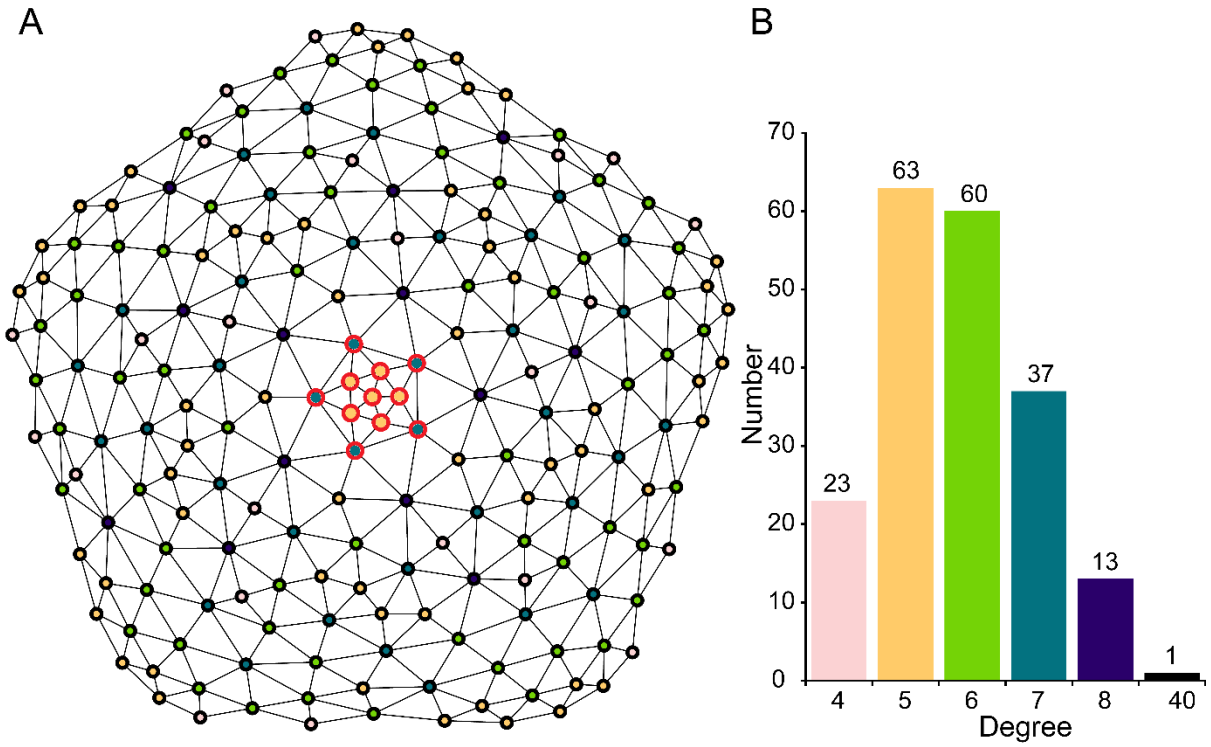

Figure 4. State spaces of possible graphs representing uintacrinoid calyx structures. (A) *Uintacrinus.* **(B)** *Marsupites.* Nested graph types are labelled on panel B, colour version: red (planar), purple (polyhedral), yellow (fullerene), magenta (pentaradial, D5h fullerene). Proportional areas of squares represent the relative numbers of possible graphs (Table 1) on a logarithmic scale. Note that if raw numbers of possible graphs (Table 1) rather than logged numbers were visually represented, areas for all graph types other than planar graphs would be invisibly small.

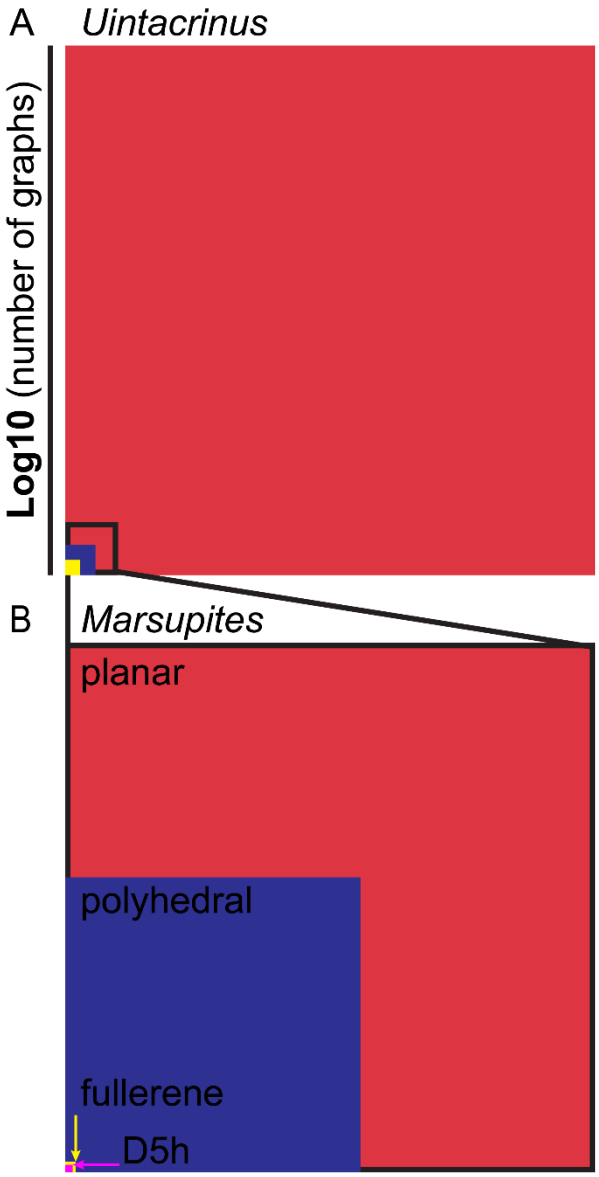

TABLES

Table 1. The number of possible graphs ($G = V, E$) representing crinoid calyx skeletal structures using vertices (V) and connecting edges (E) under a series of biophysically relevant graph constraints.

Graph condition and *corresponding biological constraint*	Possible graphs (general formula/ algorithm)	Genus	Number of vertices ($\|V\|$)	Vertex identity	Number of possible graphs (for $\|V\|$ vertices)

Planar graphs *Arrangements of plates contacting only at lateral edges*	$\leq 30.061^{\lvert V\rvert}$ (Bonichon *et al.* 2006)	*Marsupites*	17	Plates	$\leq 1.34 \times 10^{25}$
		Uintacrinus	197		$\leq 1.47 \times 10^{291}$
Polyhedral graphs *Polyhedra: 3D structures bounded by polygonal faces*	Algorithmic (Brinkmann & McKay 2007)	*Marsupites*	17		6.4×10^{12}
		Uintacrinus	197		Above computational limits: >> 1×10^{14} for $\lvert V\rvert = 18$
Fullerene graphs *Polyhedra with only pentagon and hexagon faces*	Algorithmic (Brinkmann & Dress 1997; Brinkmann & McKay 2007)	*Marsupites*	30	Plate corners	3
		Uintacrinus	390 300		Above computational limits: > 933,265,811 for $\lvert V\rvert = 300$
Pentameral fullerene graphs with mirror plane (D5h) *Fullerene structure with pentameral rotational symmetry and mirror plane*	Algorithmic (Brinkmann & Dress 1997; Brinkmann & McKay 2007)	*Marsupites*	30		1
		Uintacrinus	390 300		Above computational limits: 0 for $\lvert V\rvert = 300$

Numbers of possible graphs refer to the number of different (non-isomorphic), unlabelled graphs possible with a given number of vertices.

Acknowledgements. Research by J.F.H.C. was supported by the ELSI Origins Network (EON), with a grant from the John Templeton Foundation. We thank the curators of the Sedgwick Museum of Earth Sciences, Cambridge, Natural History Museum London and the Booth Museum, Brighton for assistance and access to specimens and equipment, as well as K. McNamara for comments on the manuscript.

686

687 **DATA ARCHIVING STATEMENT**

688 Additional supporting information is provided at the Dryad Digital Repository including

689 Tables S1-S7, Figs S1-S6 and Supplementary Computer Code:

690 429https://datadryad.org/review?doi=doi:10.5061/dryad.cc1v570.

691